Automatic particle detection in microscopy using temporal correlations

Magnus Röding[1*], Hendrik Deschout[2,3], Thomas Martens[2,3], Kristof Notelaers[4,5], Johan Hofkens[5], Marcel Ameloot[4], Kevin Braeckmans[2,3], Aila Särkkä[1], and Mats Rudemo[1]

[1] Department of Mathematical Statistics, Chalmers University of Technology and Gothenburg University, Gothenburg, Sweden
[2] Laboratory of General Biochemistry and Physical Pharmacy, Ghent University, Ghent, Belgium
[3] Center for Nano- and Biophotonics, Ghent University, Ghent, Belgium
[4] Biomedical Research Institute, Hasselt University and School of Life Sciences, Transnational University Limburg, Diepenbeek, Belgium
[5] Laboratory for Photochemistry and Spectroscopy, Department of Chemistry, Katholieke Universiteit Leuven, Heverlee, Belgium
[*] Corresponding author: roding@chalmers.se

Running title: Particle detection using temporal correlations

Abstract

One of the fundamental problems in the analysis of single particle tracking data is the detection of individual particle positions from microscopy images. Distinguishing true particles from noise with a minimum of false positives and false negatives is an important step that will have substantial impact on all further analysis of the data. A common approach is to obtain a plausible set of particles from a larger set of candidate particles by filtering using manually selected threshold values for intensity, size, shape, and other parameters describing a particle. This introduces subjectivity into the analysis and hinders reproducibility. In this paper, we introduce a method for automatic selection of these threshold values based on maximizing temporal correlations in particle count time series. We use Markov Chain Monte Carlo to find the threshold values corresponding to the maximum correlation, and we study several experimental data sets to assess the performance of the method in practice by comparing manually selected threshold values from several independent experts with automatically selected threshold values. We conclude that the method produces useful results, reducing subjectivity and the need for manual intervention, a great benefit being its easy integratability into many already existing particle detection algorithms.

Keywords: optical microscopy, fluorescence microscopy, image analysis, unsupervised learning

1 Introduction

Microscopy is gradually evolving from qualitative to quantitative. The ambition is not only to observe, but to measure. With modern-day computing resources, it is easier than ever to extract meaningful information from image data. However, this makes consistency and repeatability an urgent issue, especially since some techniques are making their way into the world of diagnostic tools and clinical applications.

Single particle tracking is becoming more widely used in cell biology, pharmacology, and various other life science fields every year (Levi and Gratton, 2010, Saxton, 2009). However, as a relatively immature technique it still comes with many obstacles (Vonesch et al., 2006). One obvious drawback is the lack of a standardized analysis workflow in the field. There are many different software solutions and algorithms being used and many researchers develop in-house solutions. As a consequence, image analysis is done very differently between experiments, see e.g. (Bornfleth et al., 1998, Boulanger et al., 2010, Genovesio et al., 2006, Ruusuvuori et al., 2010, Smal et al., 2010, Thomann et al., 2002). First steps are e.g. noise reduction, background subtraction, and other preprocessing steps, followed by identifying a set of candidate particles by e.g. simple binarization (thresholding) of the image. A common approach is to obtain a plausible set of particles from a larger set of candidate particles by filtering using manually selected threshold values for intensity, size, shape, and other parameters describing a particle candidate, see e.g. (Braeckmans et al., 2010b). How to systematically accept and reject particle candidates is a fundamental question that will have substantial impact on all further analysis of the data. In many cases, experiments are performed using dim, diffraction limited objects, such as single molecules or small nanoparticles, and low signal-to-noise and/or low signal-to-background can make this a non-trivial task. This way of identifying particles by selection of threshold values is appealing since it reduces the painstaking task of considering each candidate particle individually to the selection of a low-dimensional parameter which is physically meaningful and provides some consistency within the data set.

Computerized particle detection is not completely automatic. It involves a subjective choice of algorithms and parameters before it can start running. For example, it can be ambiguous how bright and how large a candidate particle should be to be accepted. As a consequence, there are many particle tracking studies that were performed by manually picking out a few appar-

ently interesting particles which are then manually tracked (McDonald et al., 2002). This approach is error-prone and highly subjective, and therefore dependent on the operator and can introduce considerable bias (Zimmer et al., 2002). It is evident that automation and reproducibility are important issues. How to perform the 'best' analysis is a subtle matter without a precise answer as there will always be some subjectivity. Without any subjectivity, we would only be allowed to tell a piece of image analysis software to look for 'something' and try to make sense of it. This is obviously too vague and some basic assumptions are always required. Nevertheless, it is always interesting to reduce ambiguities to a minimum, if only to improve reproducibility.

In this work, we propose a method for automatic selection of threshold values for obtaining a plausible set of particles from a larger set of candidate particles by filtering. The method is based on the theory of so called Smoluchowski processes i.e. time series of particle counts. We perform an analysis of particle count correlations and study the impact of false positives (falsely accepted noise) and false negatives (falsely rejected particles). The analysis leads to an optimality criterion used to minimize the occurrence of false positives and false negatives in a certain sense by maximizing the temporal correlation of particle counts. We use Markov Chain Monte Carlo to find the threshold values corresponding to the maximum correlation, and we study several experimental data sets to assess the performance of the method in practice by comparing manually selected threshold values from several independent experts with automatically selected threshold values and discuss the results.

2 Method

2.1 Definition of a Smoluchowski process

At the time that Einstein formulated his theory of Brownian motion (Einstein, 1905), some of his contemporaries worked on their own formulations of the same theory. Notably, M. von Smoluchowski provided an alternative viewpoint with his model for density fluctuations under equilibrium (von Smoluchowski, 1916). The setting is the following. Consider a (countably infinite) set of particles in a 'liquid suspension', say 3-dimensional space $\mathbf{R}^3$. Assume that we observe the system at time $t = 0, \Delta t, ..., n\Delta t, ...$ At all times the particles are distributed 'at random' and are thus marginally the outcome of a homogenous Poisson point process with constant density (Daley and Vere-Jones, 2003, Doob, 1953). Assume further that at any time we do not observe positions of individual particles but only the number of particles currently in a 'detection region' $\omega \subset \mathbf{R}^3$ in which particles can be observed and detected in a microscope during an experiment. Letting the positions of the particles be $\xi_p(t) \in \mathbf{R}^3$, the particle counts can be written as a sum of indicator functions by

$$X_n = X(n\Delta t) = \sum_{p=1}^{\infty} \mathbf{1}_\omega(\xi_p(t)) \tag{1}$$

where $X = X(t)$ is the particle count as a function of time with values in the state space $\mathcal{S} = \{0, 1, ...\}$ and $\mathbf{1}_\omega(\xi)$ is the indicator function of ω i.e. 1 for $\xi \in \omega$ and 0 for $\xi \notin \omega$. The particles are moving randomly. The most straightforward example is Brownian motion which is relevant for some particle characterization applications, but the motion of the particles can be much more complex. The resulting stationary time series of particle counts, which is marginally Poisson distributed, is known as a Smoluchowski process. Its mean value depends on particle concentration and the size and shape of the detection region ω. Its correlation structure depends on the size and shape of the detection region ω, the time lag Δt, and the mobility (diffusion coefficient or equivalent) of the particles.

2.2 False positives and false negatives

Assume that we observe randomly moving particles in a microscope. Due to e.g. image noise over both particles and background, clutter, diffraction

rings and other optical effects, and particle occlusion (from here on collectively denoted 'noise'), the observed particle count time series does typically not equal the true Smoluchowski process which is effectively 'hidden' in the noise. To some extent, noise will be falsely accepted and identified as particles (false positives), and particles will be falsely rejected and identified as noise (false negatives). Both effects will distort the true Smoluchowski process, see Fig. 1. The occurrence of false positives and false negatives depends on the specifics of the image analysis algorithm. In particular, threshold values for intensity, size, shape, and other parameters are crucial. The observed process will be distorted in terms of both marginal distribution and correlation structure. Intuitively, the observed particle counts will be less correlated than the true ones since false positives and false negatives will introduce additional randomness into the time series. To understand this effect, we make some simplifying assumptions. First, assume that each true particle (not knowing their respective intensity, size, shape, and other parameters) has the same probability of being falsely identified as noise, independently of all other particles both in the same frame and in other frames. Thus, the number of false negatives in a frame with $X_n = i$ true particles is binomially distributed with index i and unknown parameter ν_- (i.e. binomial thinning), $0 \leq \nu_- \leq 1$. Second, assume that the number of false positives is Poisson distributed with parameter ν_+, $0 \leq \nu_+ < \nu_+^{\max}$, where $\nu_+^{\max}$ is the maximum expected number (maximum intensity of the corresponding Poisson distribution) of false positives per frame, independent of the number of false positives in other frames and independent of the number of true particles in all frames. Third, assume that false positives and false negatives are independent of each other. Suppose that we are interested in finding a (lower) threshold value $\tau > 0$ for a single parameter P, $0 \leq P < \infty$, e.g. intensity or size, such that particle candidates for which $P \geq \tau$ are included in further analysis, and particle candidates for which $P < \tau$ are excluded. Assume that the values of P for true particles are distributed according to a probability distribution with density f_{true} and that the values of P for noise (false particles) are distributed according to a probability distribution with density f_{false}. Hence, the parameters describing the occurrence of false positives and false negatives can be expressed as functions of the threshold τ by

$$\nu_- = \int_0^\tau f_{\text{true}}(z)dz \tag{2}$$

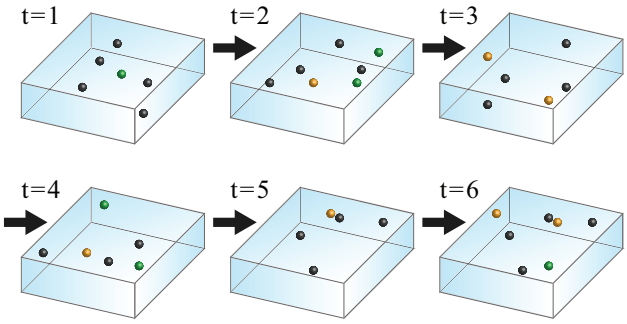

Figure 1: The Smoluchowski process i.e. the time series of particle counts is distorted by false positives and false negatives. We illustrate the process in an example with six points in time, studying what occurs within the detection region. Some particles are identified correctly (true positives, black). Some true particles are mistakenly regarded as noise (false negatives, green), and some noise is mistakenly regarded as particles (false positives, yellow). The true Smoluchowski process is the sum of the number of true positives and the number of false negatives (black + green) i.e. the series 6-6-4-5-4-5, and the observed process is the sum of the number of true positives and the number of false positives (black + yellow) i.e. the series 5-5-6-4-5-6.

and

$$\nu_+ = \nu_+^{\max} \int_\tau^\infty f_{\text{false}}(z)dz. \tag{3}$$

Typically some overlap between f_{true} and f_{false} would be expected i.e. some amount of false positives and/or false negatives is inevitable. Note that false positives and false negatives can occur simultaneously.

2.3 Correlations

Recall that if the random variable U has mean μ_U and standard deviation σ_U, and the random variable V has mean μ_V and standard deviation σ_V, the covariance of U and V is

$$\text{Cov}(U,V) = \langle (U-\mu_U)(V-\mu_V)\rangle = \langle UV\rangle - \mu_U\mu_V \tag{4}$$

where $\langle\cdot\rangle$ is the expected value. Furthermore, the (Pearson) correlation between U and V is

$$\rho(U,V) = \frac{\text{Cov}(U,V)}{\sigma_U\sigma_V}. \tag{5}$$

The (auto)correlation function is a measure of time lag-dependent correlation in a time series. For the Poisson-valued Smoluchowski process, assuming a constant mean μ and constant standard deviation $\sqrt{\mu}$ and a time lag Δt, it is defined by

$$R(m) = \frac{\langle X(t)X(t+m\Delta t)\rangle - \mu^2}{\mu}. \tag{6}$$

The correlation function $R(m)$ for a Smoluchowski process with independent particles equals the probability that a particle present in ω at time t is also present in ω at time $t + m\Delta t$ (Chandrasekhar, 1943). However, the exact nature of the correlation function of the true Smoluchowski process is of no major concern at this point.

We investigate how the correlation function of the true Smoluchowski process is distorted by false positives and false negatives. We restrict ourselves to the smallest possible time lag Δt (although the arguments hold in principle for any time lag). Suppose that the correlation of the true Smoluchowski process X_n for time lag Δt is ρ i.e.

$$\rho(X_n, X_{n+1}) = \rho. \tag{7}$$

Assume that the numbers of false positives in frames n and $n+1$ are G_n and G_{n+1} which are Poisson distributed and that the numbers of false negatives are T_n and T_{n+1} which are conditionally binomially distributed. Hence, the distorted process is formed by adding the number of false positives and subtracting the number of false negatives,

$$\tilde{X}_n = X_n - T_n + G_n \tag{8}$$

and

$$\tilde{X}_{n+1} = X_{n+1} - T_{n+1} + G_{n+1}. \tag{9}$$

We have that

$$\begin{aligned} \mathrm{Cov}(\tilde{X}_n, \tilde{X}_{n+1}) &= \\ \mathrm{Cov}(X_n - T_n + G_n, X_{n+1} - T_{n+1} + G_{n+1}) &= \\ \mathrm{Cov}(X_n - T_n, X_{n+1} - T_{n+1}), & \end{aligned} \tag{10}$$

the last step following from the fact that the number of false positives G_n is independent of both the true number of particles and the number of false negatives. Consider the first frame, n. Each of the X_n true particles are

rejected with probability ν_- and hence accepted with probability $1-\nu_-$. Therefore, the 'thinned' particle count $X_n - T_n$ can be written as a sum of X_n binary random variables, each being 1 with probability $1-\nu_-$ and 0 with probability ν_-. Reformulating Eq. 10, we obtain

$$\mathrm{Cov}(\tilde{X}_n, \tilde{X}_{n+1}) = \mathrm{Cov}\left(\sum_{i=1}^{X_n} B_{i,n}, \sum_{j=1}^{X_{n+1}} B_{j,n+1}\right) \tag{11}$$

where $B_{i,n}$, $i = 1, ..., X_n$, and $B_{j,n+1}$, $j = 1, ...X_{n+1}$, are all Bernoulli (0-1) variables with parameter $1-\nu_-$. We write the covariance explicitly using expectations and get

$$\begin{aligned} \mathrm{Cov}(\tilde{X}_n, \tilde{X}_{n+1}) &= \\ \left\langle \sum_{i=1}^{X_n} B_{i,n} \sum_{j=1}^{X_{n+1}} B_{j,n+1} \right\rangle &- \\ \left\langle \sum_{i=1}^{X_n} B_{i,n} \right\rangle \left\langle \sum_{j=1}^{X_{n+1}} B_{j,n+1} \right\rangle . & \end{aligned} \tag{12}$$

The expectations can be written as weighted sums of conditional expectations by

$$\begin{aligned} \left\langle \sum_{i=1}^{X_n} B_{i,n} \sum_{j=1}^{X_{n+1}} B_{j,n+1} \right\rangle &= \\ \sum_{I=0}^{\infty} \sum_{J=0}^{\infty} (P(X_n = I, X_{n+1} = J) &\times \\ \left\langle \sum_{i=1}^{X_n} B_{i,n} \sum_{j=1}^{X_{n+1}} B_{j,n+1} | X_n = I, X_{n+1} = J \right\rangle \Bigg) . & \end{aligned} \tag{13}$$

Given fixed values of X_n and X_{n+1}, $B_{i,n}$ and $B_{j,n+1}$ are conditionally independent for all i and j and thereby Eq. 13 can be written as

$$\begin{aligned} (1-\nu_-)^2 \sum_{I=0}^{\infty} \sum_{J=0}^{\infty} IJP(X_n = I, X_{n+1} = J) &= \\ (1-\nu_-)^2 \langle X_n X_{n+1} \rangle . & \end{aligned} \tag{14}$$

In a similar fashion, it can be found that

$$\left\langle \sum_{i=1}^{X_n} B_{i,n} \right\rangle \left\langle \sum_{j=1}^{X_{n+1}} B_{j,n+1} \right\rangle \;=$$

$$(1-\nu_-)^2\langle X_n\rangle\langle X_{n+1}\rangle. \tag{15}$$

Finally,

$$\begin{aligned}\mathrm{Cov}(\tilde{X}_n,\tilde{X}_{n+1}) &= \\ (1-\nu_-)^2(\langle X_nX_{n+1}\rangle-\langle X_n\rangle\langle X_{n+1}\rangle) &= \\ (1-\nu_-)^2\mathrm{Cov}(X_n,X_{n+1}).&\end{aligned} \tag{16}$$

Since the Smoluchowski process (both the true and the distorted process, actually) is Poisson distributed (Bingham and Dunham, 1997, Chandrasekhar, 1943), the mean and the variance of the time series are equal. Let μ be the mean and variance of X_n. Henceforth, the mean and variance of $\tilde{X}_n$ are both $(1-\nu_-)\mu+\nu_+$. Consequently, the correlation of the distorted process is

$$\tilde{\rho}=\frac{(1-\nu_-)^2\mu}{(1-\nu_-)\mu+\nu_+}\rho \tag{17}$$

Note that this expression is monotonically decreasing as a function of both ν_- and ν_+, so it attains its maximum if both these parameters are zero i.e. if no false positives or false negatives occur. The correlation approaches zero for very large thresholds τ (no particle candidates accepted) and approaches $\mu\rho/(\mu+\nu_+^{\max})$ for very small τ (all particle candidates accepted). If the densities f_{true} and f_{false} have disjoint supports than the maximum value will be ρ, otherwise it will be lower.

2.4 Threshold selection method

By preprocessing a set of particle candidates is obtained. The number of particle candidates per frame forms a time series χ_n. It is assumed that all true particles are included as particle candidates (provided that the preprocessing is liberal in the sense that no false negatives are introduced) and thereby that $X_n\leq\chi_n$ for all n. By a suitable selection of threshold value(s), χ_n is to be divided into a set of accepted particles forming a time series $\hat{X}_n$ and a set of rejected particles. The basis of the proposed method is to select threshold values for which the correlation of $\hat{X}_n$ is maximized. In the idealized case that f_{true} and f_{false} do not overlap at all, maximizing the correlation corresponds to removing all false positives and false negatives. We note without derivation that, using the same argument as above, it can be found that the

correlation of the time series of rejected particle counts is

$$\frac{\nu_-^2 \mu}{\nu_- \mu + \nu_+^{\max} - \nu_+} \rho. \tag{18}$$

This correlation approaches $\mu\rho/(\mu + \nu_+^{\max})$ for very large τ and approaches zero for very small τ. If the densities f_{true} and f_{false} have disjoint supports then this implies that the candidate particles are divided into one 'maximally correlated' and one 'minimally correlated' set. In general, however, the two sets are rather 'maximally correlated' and 'less correlated'.

The correlation of accepted particles can be expressed in terms of sensitivity and specificity. Let TP be true positives, FP be false positives, TN be true negatives, and FN be false negatives. Recall that

$$\text{sensitivity} = \frac{\#\text{TP}}{\#\text{TP} + \#\text{FN}} \tag{19}$$

and

$$\text{specificity} = \frac{\#\text{TN}}{\#\text{TN} + \#\text{FP}}. \tag{20}$$

Hence, we obtain that

$$\tilde{\rho} = \frac{\text{sensitivity}^2 \times \mu}{\text{sensitivity} \times \mu + \nu_+^{\max} \times (1 - \text{specificity})} \rho. \tag{21}$$

Maximizing the correlation hence corresponds to simultaneously maximizing sensitivity and specificity in the certain sense described above. Accepting and rejecting particle candidates can be thought of as an unsupervised, binary classification problem with Eq. (21) implicitly defining the loss function.

In practice, maximizing the correlation is performed using a Markov Chain Monte Carlo (MCMC) optimization scheme called (constant-temperature) simulated annealing (Kirkpatrick et al., 1983, Černý, 1985). After finding a random feasible vector by rejection sampling, random jumps are made in the parameter space. Whether to make a jump or not is determined by the values c and c^* for the correlations in the time series corresponding to the old and the new parameter vector, respectively. The new parameter vector c^* replaces the old parameter vector c if

$$U < e^{-(c-c^*)/T} \tag{22}$$

where U is a uniformly distributed random number in $[0, 1]$ and T is the 'temperature' that controls the acceptance rate. Otherwise the old parameter vector c is kept. We let a large number of these Markov chains explore the parameter space in parallel. The parameters yielding the largest correlation are stored. The algorithm is implemented in Matlab R2010b (MathWorks, Natick, MA).

3 Results

3.1 Theoretical example

We illustrate threshold selection in a theoretical example. Suppose that we are interested in finding a (lower) threshold value $\tau > 0$ for some single parameter P, $0 \leq P < \infty$ such that particle candidates for which $P \geq \tau$ are included in further analysis, and particle candidates for which $P < \tau$ are excluded. The values of P for true particles are distributed according to a probability distribution with density f_{true} and that the values of P for noise (false particles) are distributed according to a probability distribution with density f_{false}. Both distributions are log-normal in this example. The ratio $\mu/\nu_+^{\max}$ is 1/3. The parameters ν_- and ν_+ can thus be exactly determined as a function of the threshold τ using Eqs. (2) and (3), and the correlation then theoretically computed using Eq. (17). The distributions of the property P among the true particles and the false particles are shown in Fig. 2, with an overlap that will inevitably yield false positives and/or false negatives regardless of the value of τ. The value of the correlation as a function of τ is shown in Fig. 3. The figure indicates that at the optimal threshold, the correlation is still substantially smaller than for the original process. This is indeed an effect of the overlap between f_{true} and f_{false}. In Fig. 4, the receiver operating characteristic (ROC) curve (Egan, 1975) is shown, where the set of all possible thresholds $\tau \in [0, \infty)$ are mapped into a curve in specificity-sensitivity space going from $(1, 0)$ for $\tau = \infty$ (all particle candidates rejected) to $(0, 1)$ for $\tau = 0$ (all particle candidates accepted).

3.2 Experimental study

For evaluation, manual selections of threshold values based on previous experience and 'best practice' are made by three experts. Three different sets of videos as described below are analyzed using custom developed software to detect individual particles, see (Braeckmans et al., 2010a). Prior to filtering particle candidates by threshold selection, all three experts agree on suitable preprocessing settings. This involves several steps. First, the nonuniform background is removed as much as possible by using so-called unsharp filtering. Second, median filtering is applied for noise reduction. Third, a set of objects is identified by binarization (intensity thresholding) of the images. Fourth, these objects or particle candidates are measured individually

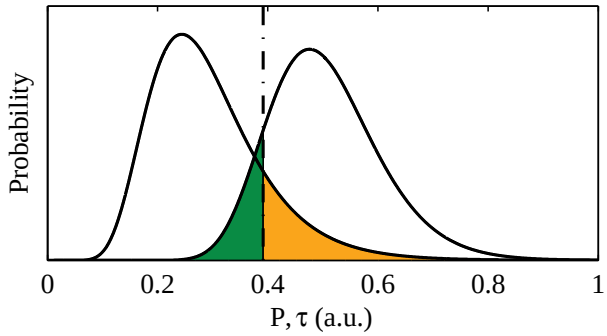

Figure 2: A theoretical example where both f_{true} and f_{false} are log-normal. The optimal threshold is indicated by the vertical dashed line. False positives (yellow) and false negatives (green) are indicated.

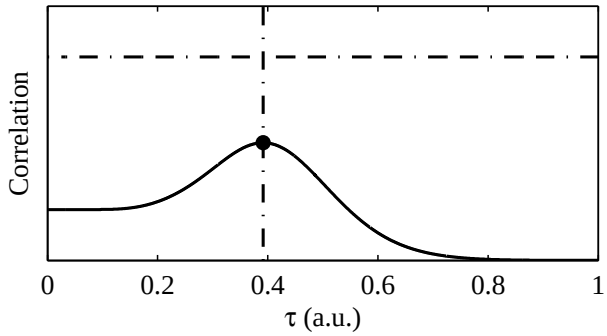

Figure 3: The correlation as a function of the threshold τ. The optimal threshold selection yielding the highest correlation is indicated by the vertical dashed line and the black dot. We note that correlation approaches zero for very large τ and approaches $\mu/(\mu + \nu_+^{\max}) = 1/4$ for very small τ. Notably, the maximal correlation is substantially smaller than for the original process, indicated by the horizontal dashed line.

in terms of different properties. In this experimental evaluation surface size (in pixels), contrast (signal-to-background ratio), and standard deviation of radius (used to quantify shape i.e. deviation from circularity) are used. The stationarity assumption holds given that each video is sufficiently short to avoid substantial photobleaching. After this preprocessing stage, the experts (and the automatic algorithm) work individually to select a set of thresholds for these three properties to reduce the (typically large) set of particle can-

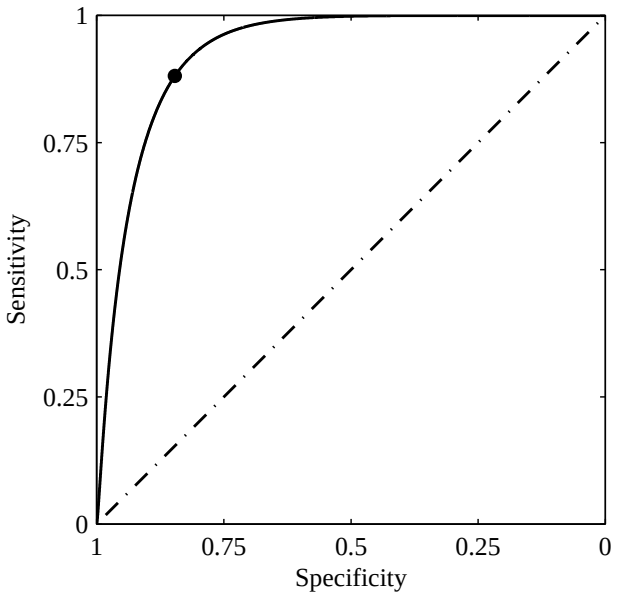

Figure 4: The receiver operating characteristic (ROC) curve, where the set of all possible thresholds $\tau \in [0, \infty)$ are mapped onto a curve in specificity-sensitivity space going from $(1, 0)$ for $\tau = \infty$ to $(0, 1)$ for $\tau = 0$. The sensitivity and specificity for the optimal threshold are indicated by the black dot.

didates to a smaller set of accepted particles. This produces a comparison in a realistic setting.

Three different experimental data sets were studied for the evaluation of the method: (i) Model nanospheres in water, (ii) liposomes in blood, and (iii) single molecules in cell membrane. For both the nanospheres and liposomes data, single particle tracking experiments were carried out on a custom-built laser widefield epi-fluorescence microscope setup that is described elsewhere in more detail (Braeckmans et al., 2010a). Briefly, a 100 mW Calypso 491 nm (Cobolt, Solna, Sweden) solid state laser was used for illumination. The microscope was a Nikon TE2000-E (Nikon Belux, Brussels, Belgium) with a Nikon Plan Apochromat 100x NA1.4 oil immersion objective lens. Time-lapse movies were recorded with a Cascade II:512 EMCCD camera (Roper Scientific, Tucson, USA). A pair of achromat lenses was placed in between the camera and microscope side port for an extra 2x magnification of the image on the CCD chip. High-speed movies were recorded using the Nikon Ele-

ments R imaging software. For the nanospheres data, Tetraspeck polystyrene nanosphere beads of nominal size 200 nm (Invitrogen, Merelbeke, Belgium) were tracked making use of a green (505 nm excitation peak, 515 nm emission peak) fluorescent label. The beads were diluted in water to a concentration of approximately 10^9 part/ml. A microscope sample was prepared by applying 5 μl of the bead suspension between a microscope slide and a cover glass with a double-sided adhesive Secure-Seal Spacer of 120 μm thickness (Molecular Probes, Leiden, The Netherlands) in between. The frame rate was approximately 40 fps. See (Deschout et al., 2012) for more details. The liposome data were taken from a previous study where liposomal drug carriers were intravenously injected into the lateral tail vein of three 8-week old Sprague-Dawley rats (Elevage Janvier, Le Genest Saint Isle, France) and tracked 5 min after injection. 200 μl of liposome suspension was injected. Cationic liposomes were made out of equimolar amounts of 1,2-dioleoyl-3-trimethylammoniumpropane (DOTAP), a cationic lipid, and 1,2-dioleoyl-*sn*-glycero-3-phosphoethanolamine (DOPE), a neutral fusogenic lipid (Avanti Polar Lipids, Alabaster, AL, USA). The liposomes were functionalized by adding 1,2-distearoyl-*sn*-glycero-3-phosphoethanolamine-N-[methoxy(polyethylene glycol)2000] (DSPE-PEG). The frame rate was approximately 40 fps. See (Braeckmans et al., 2010a) for further details. For the single molecules data, single particle tracking measurements were carried out on a setup also described in detail elsewhere (Kim et al., 2009). Glycine receptors α3K were dyed with Alexa 647 fluorophores and were imaged with excitation from a 60 mW 642 nm diode laser (Excelsior 642, Spectra-Physics, Santa Clara, CA), a Z647RDC DC and a 665LP emission filter (Chroma, Rockingham, VT). Live cells were kept at 37°C through the use of a commercial stage incubator (Pecon, Erbach, Germany). The frame rate was approximately 10 fps. See (Notelaers et al., 2012) for further details. Movies of parts of the different data sets with the particles detected using the automatic method are appended as supporting information.

Assuming (under the null hypothesis) that the automatic threshold selection is 'comparable' to the manual ones, all four sets of accepted particles can be compared against each other. First, we do this one-on-one i.e. evaluating all four and using the opposing three as reference one at a time. Second, we do this one-on-three i.e. evaluating all four and using a combination of the opposing three as a single reference. Sensitivity and specificity are used as performance measures when comparing the automatic (A) and the manual (M1, M2, and M3) selections. We also study the obtained correlations of the

extracted time series as well as making direct visual comparison between the different sets of accepted particles.

Results for the one-on-one comparison for all data sets are shown in Tab. 1. Each row corresponds to a reference selection of particles and each column corresponds to an evaluated selection of particles (i.e. in the first row all selections are compared to M1). There is no overall emerging pattern for neither sensitivity nor specificity. The difference between A and any of M1, M2, and M3 can be smaller and larger than between any two of M1, M2, and M3. One obvious conclusion is that whereas M1 and M2 appear quite similar, M3 deviates clearly from both. This can be attributed to differences in experiences and habits and hence differences in the operators' subjective bias. One should also bear in mind that there is no right answer since, indeed, being more liberal in the selection of thresholds i.e. including more particles effectively results in a larger axial size of the detection region whereas being more conservative i.e. including less particles effectively results in a smaller axial size (Jaqaman et al., 2008, Röding et al., 2011, 2013). One could say that in reality, the aim is not to extract *the* Smoluchowski process but rather to find a suitable and 'accessible' choice from a whole family of Smoluchowski processes, parametrized by the axial size of the detection region. Studying Tab. 2, where the references have been constructed by including particles present in all of the three opposing selections, it is somewhat easier to rank the four selections, and it appears once again that M1 and M2 are quite similar. Notably, M3 stands out as conservative in the nanospheres in water data set, and A stands out as conservative in the liposomes in blood data set. The total number of accepted particles as shown in Tab. 3 sheds some additional light on this. The automatic selection A goes from quite liberal to very conservative between data sets, especially compared to M3. On the other hand, for example, visual inspection indicates that M3 is very liberal on the liposomes in blood data set. To some extent, A appearing relatively 'bad' can be explained by the fact that M1 and M2 are quite similar, since this has a substantial impact on the analysis. Manual operators being conservative or liberal in their accepting and rejecting particles can be understood as them having different goals with the analysis regarding quantitative analysis, e.g. estimation of diffusion coefficients, or qualitative analysis, e.g. observing different types of mobility. Furthermore, human operators tend to think a step ahead unlike automatic algorithms. In this case, it means to take into account e.g. the fact that false positives can be removed to some extent in postprocessing by removing short trajectories, as

they are prone to be mistakes (Braeckmans et al., 2010b, Jaqaman et al., 2008). On the other hand, it is of some interest not to introduce bias by removing short trajectories. Anyhow, it is clear from Tabs. 1, 2, and 3 that not even experts agree on what the best selection of thresholds is.

Since the method is based on correlation maximization, it is of some interest to compare the obtained correlations for M1, M2, M3, and A. Considering Tab. 4 we note, obviously, that the correlation of the counts of accepted particles is the largest for A. However, we note that the correlation is rather close to the maximum attained value for M1, M2, and M3. This is not surprising, though, and it indicates that striving toward a highly correlated data set is an intuitive way of finding good thresholds thus giving some credibility to the method. It is important to stress here that the actual value of the attained correlation cannot be taken as a measure of 'goodness of fit', since it is dependent on the mobility of particles, the size and shape of the detection region ω and the frame rate. Therefore, only relative values of the correlation are relevant in the current setting. We note without proof that a highly correlated process corresponds to long trajectories among the observed particles.

To visualize the different threshold selections, we compare realizations of particle count time series for particles accepted by M1, M2, M3, and A in Fig. 5 for part of the nanospheres in water data set. We see that the general behavior of the four time series is quite similar, although they all fluctuate up and down somewhat compared to each other. Studying a single frame of the liposomes in blood data set as shown in Fig. 6 it can be seen that all four selections are self-consistent as is expected considering that the problem is regularized by reducing the dimensionality to a few parameters, and that they range from the most conservative (A) to the most liberal (M3). Both M1 and M2 are here quite similar to A.

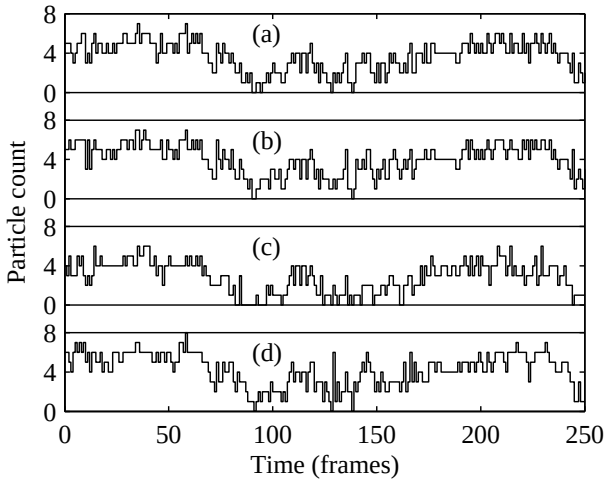

Figure 5: Time series of counts of accepted particles for (a) M1, (b) M2, (c) M3, and (d) A, for part of the nanospheres in water data set.

4 Discussion and conclusion

In this paper, we propose a method for automatic selection of threshold values for intensity, size, shape, and other parameters used for particle detection in image analysis of microscopy images. The analysis is based on the theory of Smoluchowski processes or particle count time series and an analysis of the impact on the correlation structure of false positives and false negatives. By introducing some simplifying assumptions about the occurrence of false positives and false negatives, a simple model leads to an optimality criterion demonstrating how to find the best threshold in a certain sense. The principle is general and should hold for any preprocessing scheme and any set of physically plausible threshold values to be selected.

We use several experimental data sets to evaluate the performance of the method in practice by comparing manually selected threshold values from several independent experts with automatically selected threshold values. The results are promising and indicate that the automatic threshold selection is competitive although, as discussed, there is no single Smoluchowski process which is the best, but rather a family of Smoluchowski processes depending on the axial size of the detection region, determining how far from the focal plane particles can be detected. Therefore, when different sets of accepted particles are liberal or conservative relative to each other, it is a difficult

task to quantify what best really means. Since the automatic algorithm is only focused on particle positions, and manual operators tend to think in terms of finding credible particle trajectories in postprocessing, results can be different.

Nevertheless, the algorithm proposed here provides a framework for consistent and automatic threshold selection that can assist in reducing subjectivity and the need for manual intervention. It is theoretically and computationally simple and can easily be parallelized to analyze large numbers of data sets for high throughput studies, a great benefit being its easy integratability into many already existing particle detection algorithms.

Regarding further work, it is of some interest to understand how mobility, time lag, and different experimental setups overall affect the performance of this method. For example, sources of error and the impact of several factors is unknown e.g. the amount of noise i.e. the choices made in preprocessing, the correlations in the noise versus the correlations in the true process, and possible non-stationarity of the time series due to e.g. substantial photobleaching. Additionally, although some particle candidates are very clearly true particles and others are very clearly noise, some are uncertain i.e. close to the threshold. It could be offered to the user to introduce manual corrections after the analysis on particle candidates that are uncertain. Also, constraints could be manually defined prior to analysis to force certain particle candidates to be included or excluded. Last, it is possible that other optimality criteria could be found using other measures than Pearson correlation, in turn yielding other balances between false positives and false negatives that could be beneficial. It is important to emphasize that the results produced are only optimal with regard to a certain loss function, whereas the loss function itself may not be 'optimal' with regard to the subject-matter. For example, slowly moving particles contribute more to the correlation of the corresponding particle count time series than quickly moving particles, which may lead the algorithm toward rejecting quickly moving particles.

In conclusion, the proposed method is theoretically simple and transparent and provides a simple means of automatic threshold selection, reducing the need for manual intervention in image analysis of microscopical data. This is important for the sake of obtaining credible, representative, and reproducible results. A great benefit is the method's easy integratability into many already existing particle detection algorithms.

Acknowledgments

Some of the computations were performed on C3SE (Chalmers Centre for Computational Science and Engineering) computing resources. Hendrik Deschout is a doctoral fellow of the Institute for the Promotion of Innovation through Science and Technology in Flanders (IWT), Belgium. This work has been carried out with financial support from the Swedish Foundation for Strategic Research (SSF) through Gothenburg Mathematical Modelling Center (GMMC), from the VINN Excellence Centre SuMo Biomaterials, the BIOSUM research school, and the Funds for Scientific Research, Flanders (project G.0197.11).

References

N. Bingham and B. Dunham. Estimating diffusion coefficients from count data: Einstein-Smoluchowski theory revisited. *Ann Inst Statist Math*, 49: 667–679, 1997.

H. Bornfleth, K. Satzler, R. Eils, and C. Cremer. High-precision distance measurements and volume-conserving segmentation of objects near and below the resolution limit in three-dimensional confocal fluorescence microscopy. *Journal of Microscopy*, 189:118–136, 1998.

J. Boulanger, A. Gidon, C. Kervran, and J. Salamero. A patch-based method for repetitive and transient event detection in fluorescence imaging. *PloS one*, 5(10):e13190, 2010.

K. Braeckmans, K. Buyens, W. Bouquet, C. Vervaet, P. Joye, F. D. Vos, L. Plawinski, L. Doeuvre, E. Angles-Cano, N. Sanders, J. Demeester, and S. C. D. Smedt. Sizing nanomatter in biological fluids by fluorescence single particle tracking. *Nano Lett*, 10:4435–4442, 2010a.

K. Braeckmans, D. Vercauteren, J. Demeester, and S. de Smedt. Single particle tracking. In E. Diaspro, editor, *Nanoscopy multidimensional optical fluorescence microscopy*. Taylor and Francis, 2010b.

S. Chandrasekhar. Stochastic problems in physics and astronomy. *Rev Mod Phys*, 15(1):1–89, 1943.

D. Daley and D. Vere-Jones. *An introduction to the theory of point processes. Volume I: Elementary theory and methods*. Springer, 2003.

H. Deschout, K. Neyts, and K. Braeckmans. The influence of movement on the localization precision of sub-resolution particles in fluorescence microscopy. *Journal of Biophotonics*, 109:97–109, 2012.

J. Doob. *Stochastic processes*. Wiley, 1953.

J. Egan. *Signal Detection Theory and ROC Analysis*. Series in Cognitition and Perception. Academic Press, 1975.

A. Einstein. Über die von der molekulärkinetischen Theorie der Wärme gefordete Bewegung von in ruhenden Flüssigkeiten suspendierten Teilchen

(On the movement of small particles suspended in stationary liquids required by the molecular-kinetic theory of heat). *Annalen der Physik*, 17: 549–560, 1905.

A. Genovesio, T. Liedl, V. Emiliani, W. Parak, M. Coppey-Moisan, and J.-C. Olivo-Marin. Multiple particle tracking in 3-d+t microscopy: Method and application to the tracking of endocytosed quantum dots. *IEEE Transactions on Image Processing*, 15:1062–1070, 2006.

K. Jaqaman, D. Loerke, M. Mettlen, H. K. S. G. S. Schmid, and G. Danuser. Robust single-particle tracking in live-cell time-lapse sequences. *Nat Methods*, 5:695–702, 2008.

T. Kim, H. Uji-i, M. Möller, B. Muls, J. Hofkens, and U. Alexiev. Monitoring the interaction of a single g-protein key binding site with rhodopsin disk membranes upon light activation. *Biochemistry*, 48:3801–3803, 2009.

S. Kirkpatrick, C. Gelatt, and M. Vecchi. Optimization by simulated annealing. *Science*, 220:671–680, 1983.

V. Levi and E. Gratton. Three-dimensional particle tracking in a laser scanning fluorescence microscope. In C. Brächle, D. Lamb, and J. Michaelis, editors, *Single particle tracking and single molecule energy transfer*. Wiley, 2010.

D. McDonald, M. Vodicka, G. Lucero, T. Svitkina, and G. Borisy. Visualization of the intracellular behavior of HIV in living cells. *Journal of Cell Biology*, 159:441–452, 2002.

K. Notelaers, N. Smisdom, S. Rocha, D. Janssen, J. Meier, J.-M. Rigo, J. Hofkens, and M. Ameloot. Ensemble and single particle fluorimetric techniques in concerted action to study the diffusion and aggregation of the glycine receptor $\alpha 3$ isoforms in the cell plasma membrane. *Biochimica et Biophysica Acta*, 1818:3131–3140, 2012.

M. Röding, H. Deschout, K. Braeckmans, and M. Rudemo. Measuring absolute number concentrations of nanoparticles using single-particle tracking. *Phys Rev E*, 84:031920, 2011. doi: 10.1103/PhysRevE.84.031920.

M. Röding, H. Deschout, K. Braeckmans, and M. Rudemo. Measuring absolute nanoparticle number concentrations from particle count time series. *Journal of Microscopy*, 251:19–26, 2013.

P. Ruusuvuori, T. Äijö, S. Chowdhury, C. Garmendia-Torres, J. Selinummi, M. Birbaumer, A. Dudley, L. Pelkmans, and O. Yli-Harja. Evaluation of methods for detection of fluorescence labeled subcellular objects in microscope images. *BMC Bioinformatics*, 11(1):248–264, 2010.

M. Saxton. Single-particle tracking. In T. Jue, editor, *Fundamental concepts in biophysics*. Springer, 2009.

I. Smal, M. Loog, W. Niessen, and E. Meijering. Quantitative comparison of spot detection methods in fluorescence microscopy. *IEEE Transactions on Medical Imaging*, 29(2):282–301, 2010.

D. Thomann, D. Rines, P. Sorger, and G. Danuser. Automatic fluorescent tag detection in 3d with super-resolution: Application to the analysis of chromosome movement. *Journal of Microscopy*, 208:49–64, 2002.

V. Černý. Thermodynamical approach to the traveling salesman problem: An efficient simulation algorithm. *Journal of optimization theory and applications*, 45:41–51, 1985.

M. von Smoluchowski. Drei Vorträge über Diffusion, Brownsche Molekularbewegung und Koagulation von Kolloidteilchen (Three lectures on diffusion, Brownian molecular motion and coagulation of colloidal particles). *Physikalische Zeitschrift*, 17:557–571 and 587–599, 1916.

C. Vonesch, F. Aguet, J.-L. Vonesch, and M. Unser. The colored revolution of bioimaging. *IEEE Signal Processing Magazine*, 23:20–31, 2006.

C. Zimmer, E. Labruyere, V. Meas-Yedid, N. Guillen, and J.-C. Olivo-Marin. Segmentation and tracking of migrating cells in videomicroscopy with parametric active contours: a tool for cell-based drug testing. *IEEE Transcations on Medical Imaging*, 21:1212–1221, 2002.

Table 1: Results one-on-one evaluation

Nanospheres in water

Sensitivity

	M1	M2	M3	A
M1	-	1.0000	0.7414	0.9540
M2	0.9087	-	0.6750	0.9139
M3	0.9981	1.0000	-	0.9846
A	0.8301	0.8751	0.6364	-

Specificity

	M1	M2	M3	A
M1	-	0.9947	0.9999	0.9897
M2	1.0000	-	1.0000	0.9924
M3	0.9865	0.9813	-	0.9782
A	0.9975	0.9949	0.9994	-

Liposomes in blood

Sensitivity

	M1	M2	M3	A
M1	-	0.9988	1.0000	0.6223
M2	0.6123	-	1.0000	0.3854
M3	0.4927	0.8037	-	0.3120
A	0.9827	0.9927	1.0000	-

Specificity

	M1	M2	M3	A
M1	-	0.9597	0.9343	0.9993
M2	0.9999	-	0.9735	0.9997
M3	1.0000	1.0000	-	1.0000
A	0.9765	0.9375	0.9130	-

Single molecules in cell membrane

Sensitivity

	M1	M2	M3	A
M1	-	1.0000	0.8531	0.9619
M2	0.8807	-	0.7688	0.9205
M3	0.8337	0.8531	-	0.8075
A	0.8375	0.9101	0.7194	-

Specificity

	M1	M2	M3	A
M1	-	0.9449	0.9308	0.9241
M2	1.0000	-	0.9353	0.9556

Table 2: Results for one-on-three evaluation

Nanospheres in water

Sensitivity

M1	M2	M3	A
0.9981	1.0000	0.7652	0.9846

Specificity

M1	M2	M3	A
0.9859	0.9807	0.9993	0.9781

Liposomes in blood

Sensitivity

M1	M2	M3	A
0.9881	0.9981	1.0000	0.6219

Specificity

M1	M2	M3	A
0.9764	0.9371	0.9123	0.9992

Single molecules in cell membrane

Sensitivity

M1	M2	M3	A
1.0000	1.0000	0.8590	0.9685

Specificity

M1	M2	M3	A
0.9340	0.8825	0.9211	0.8763

Table 3: Total number of accepted particles

Nanospheres in water

M1	M2	M3	A
7776	8557	5776	8936

Liposomes in blood

M1	M2	M3	A
12518	20420	25407	7927

Single molecules in cell membrane

M1	M2	M3	A
232010	263432	237387	266459

Table 4: Correlation of counts for accepted particles

Nanospheres in water

M1	M2	M3	A
0.7266	0.6929	0.7051	0.7634

Liposomes in blood

M1	M2	M3	A
0.5936	0.5830	0.5740	0.6611

Single molecules in cell membrane

M1	M2	M3	A
0.9059	0.9199	0.8816	0.9461

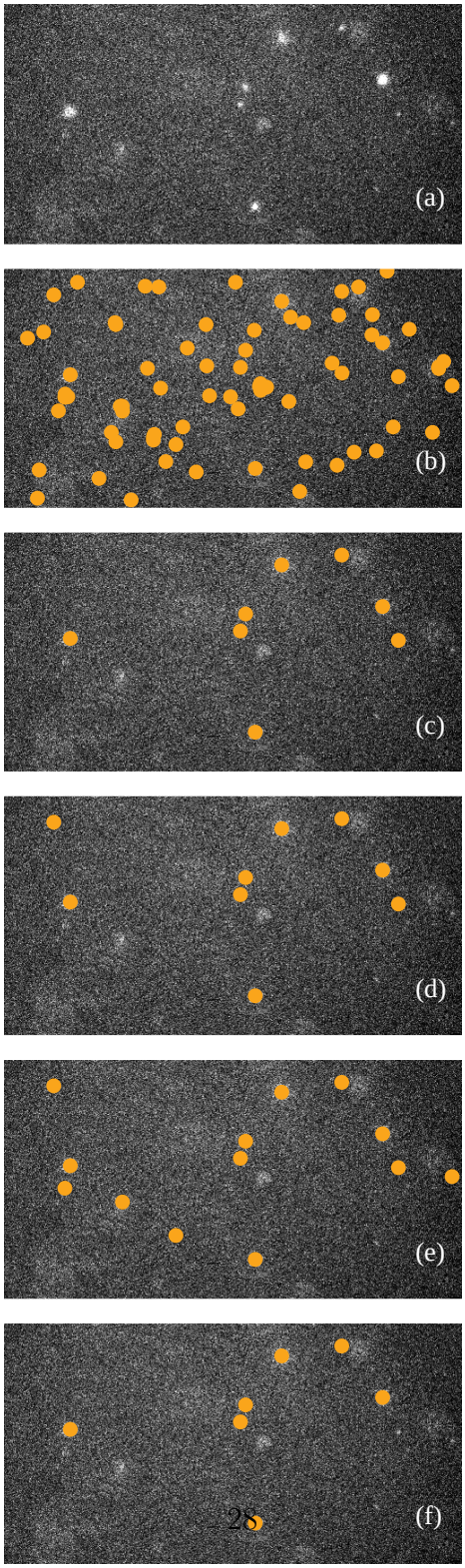

Figure 6: Comparison of different selection rules of particles in one image from the liposomes in blood data set, showing (a) original microscope image (contrast enhanced), (b) all candidate particles after the preprocessing stage, and selections of (c) M1, (d) M2, (e) M3, and (f) A using the proposed method.